Carbohydrate Polymers 101 (2014) 684–691

Contents lists available at ScienceDirect

Carbohydrate Polymers

journal homepage: www.elsevier.com/locate/carbpol

Adsorptional removal of methylene blue by guar gum–cerium (IV) tungstate hybrid cationic exchanger

V.K. Gupta [a,*], Deepak Pathania [b], Pardeep Singh [b], Amit Kumar [b], B.S. Rathore [b]

[a] Department of Chemistry, Indian Institute of Technology, Roorkee 247667, India
[b] School of Chemistry, Shoolini University, Solan 173212, Himachal Pradesh, India

ARTICLE INFO

Article history:
Received 15 August 2013
Received in revised form
21 September 2013
Accepted 27 September 2013
Available online 5 October 2013

Keywords:
Hybrid ion exchanger
Characterization
Methylene blue
Adsorption
Kinetics

ABSTRACT

Guar gum–cerium (IV) tungstate nanocomposite (GG/CTNC) cationic exchanger was synthesized using simple sol gel method. The GG/CTNC was characterized using X-ray diffraction (XRD), Fourier transmission infrared spectroscopy (FTIR), scanning electron microscopy (SEM) and energy dispersive X-ray spectrophotometer (EDX). The XRD studies confirmed amorphous and fibrous in nature of GG/CTNC. The high percentage of oxygen in the nanocomposite material confirmed the functionality tungstate (WO_4^-). The ion exchange capacity of GG/CTNC for Na^+ ion was observed to be 1.30 meq g^{-1}. The hybrid exchanger was used as potential adsorbent for the removal of methylene blue (MB) from aqueous system. The correlation coefficients value indicated a good fit of monolayer Langmuir model to the adsorption of methylene blue onto GG/CTNC. The adsorption kinetic study revealed that the adsorption process followed the pseudo second order kinetic. The Gibbs free energy (ΔG) values confirmed the spontaneous nature of adsorption process.

1. Introduction

The fast industrial development throughout world has significantly increased the production of wastewater from various industries such as, textile, paper, paint, and dyestuffs consume; as a consequence toxic synthetic dyes are discharged into water bodies. The discharged dyes degrade the water quality and may cause adverse effect on human health due to toxic, mutagenic and carcinogenic nature (Gupta & Ali, 2008; Gupta, Agarwal, & Saleh, 2011; Gupta, Jain, & Varshney, 2007; Gupta, Mittal, Malviya, & Mittal, 2009; Gupta, Rastogi, & Nayak, 2010; Gupta, Pathania, Agarwal, & Singh, 2012; Mittal, Gupta, Malviya, & Mittal, 2008; Mittal, Mittal, Malviya, Kaur, & Gupta, 2010). The synthetic dyes are difficult to treat, since these are resistant to biological oxidation/reduction, and stable to oxidizing agents. The application of conventional methods like coagulation, flocculation, precipitation, membrane separation, solvent extraction and adsorption, does not treat industrial dye-effluent efficiently (Vilhera, Goncalves, & Mota, 2004). In practice, no single process provides adequate treatment and combination of different process has been often used to improve the water quality in most greener and economic way. It is now well recognized that bio-adsorbent are gaining importance as effective and economic methods for wastewater remediation. A large number of non-conventional bio-adsorbents such as fungal or bacterial biomass or biopolymers have been employed to remove toxic metals and dyes from aqueous phase (Constantin et al., 2013; Zhao, Zeng, Li, et al., 2012a; Zhao, Zeng, Hu, et al., 2012b). The bio-adsorbent are low-cost, harmless and abundantly available (Constantin et al., 2013; Yang et al., 2012). However, lower stability, difficulty in separation from aqueous phase and low recovery after desorption were the major limitations for large scale applicability of bio-absorbents (Gupta et al., 2011, 2012).

Organic–inorganic nanocomposite materials are of importance because of their multifunctionality owing to a combination of different compounds incorporated. Recently, TiO_2, BiOCl, Fe_2O_3, CuS and ZnO based bio-nanocomposites have been used for dyes and metal removal from wastewater (Dong, Sun, Min, Wu, & Lee, 2012; Gupta et al., 2012; Huang & Chen, 2009; Virkutyte, Jegatheesan, & Varma, 2012). Nowadays, bio-material based nanocomposites have drawn considerable attention because of their low-cost, easy processability, high-volume application, renewable nature and possibility of recycling. There are several research efforts reporting the bio-composite with carbon nanotubes, lignin and lumiscent CdS (Nevarez et al., 2011; Park & Kadla, 2012; Yang et al., 2012). Guar is a naturally occurring polysaccharide extracted from the beans of the guar gum plant. It is used as environmental-friendly thickener to control visco-elasticity in food, personal care and oil recovery industries. Cerium (IV) derivates represent inorganic ion exchangers of tetravalent metal acid salts class. It has shown excellent adsorption ability for heavy metal due to its high selectivity, high thermal stability and absolute insolubility in water (Semischenko,

* Corresponding author. Fax: +91 1332273560.
E-mail addresses: vinodfcy@gmail.com, vinodfcy@iitr.ernet.in (V.K. Gupta), dpathania74@gmail.com (D. Pathania).

0144-8617/$ – see front matter © 2013 Elsevier Ltd. All rights reserved.
http://dx.doi.org/10.1016/j.carbpol.2013.09.092

Stepanenko, Gulina, & Tolstoi, 2011). Brigante et al. investigated adsorptional behavior of cerium (IV) oxide the separation of antibiotic minocyline (Brigante & Schulz, 2012). Sivashankar et al. synthesized cerium tailored carbon and studied its adsoptional behavior for fluoride removal from drinking water (Sivasankar, Murugesh, Rajkumar, & Darchen, 2013). Semischenko et al. prepared and investigated physico-chemical properties of cerium (IV) tungstate nanolayers (Semischenko et al., 2011). However major disadvantage of synthetic inorganic ion exchangers is the difficulty in preparing granulated materials with high adsorption capacity for effective removal of organic pollutants from wastewater. Hybrid nanocomposites are recently the materials of interest due to their multifunctionality involving the combination of different compounds.

To best of our knowledge, no data are available on the adsorption activity of guar gum–cerium (IV) tungstate (GG/CTNC) for methylene blue removal from aqueous phase. The present work deals with sol-gel preparation of guar gum–cerium (IV) tungstate composite. The ion exchange behavior of GG/CTNC will be investigated for adsorption of different metal ions. The adsorptional activity of GG/CTNC was also utilized for the removal of methylene blue. GG/CTNC was characterized by scanning electron transmission (SEM), transmission electron microscopy (TEM), energy dispersive X-ray (EDX) and X-ray diffraction (XRD) spectral techniques.

2. Experimental

2.1. Materials and methods

Ceric ammonium nitrate, sodium tungstate and methylene blue were purchased from Sigma-Aldrich, India and used without further purification. Guar gum was obtained from Rama industries, India. All other chemicals and reagents used were of analytical reagent grade. All the solutions were prepared in double distilled water.

2.2. Preparation of guar gum–cerium (IV) tungstate (GG/CTNC)

Guar gum based nanocomposite was synthesized using ambient sol gel method. In first step, 0.1 M ceric ammonium nitrate solution and 0.1 M sodium tungstate solution were gradually mixed with continuous stirring at pH 2. After complete addition, the mixture was stirred for 5 h to obtain cerium (IV) tungstate precipitates. The precipitates were washed with distilled water and dried at 70 °C. In next step, guar gum was prepared by dissolving 0.25 g of guar powder in the distillated water and ethanol in molar ratio of 2:1 with continuous stirring at room temperature. The resultant mixture was allowed to stand for 24 h with occasional shaking in the mother liquor for digestion. The precipitates were separated by filtration and washed with demineralized water several times to remove excess of the reagents. The obtained precipitates were kept in 0.1 M HNO_3 solution for 24 h to convert into H^+ form. The precipitates were filtered and washed with demineralized water to remove any excess of acid and finally dried in oven at 80 °C.

2.3. Batch equilibrium experiments

Adsorption experiments were performed using standard batch method. In this method, stipulated amount of adsorbent was added to 100 mL of MB solution of placed in a set of 250 mL glass stopper Erlenmeyer flasks. In each case, the mixture was agitated in a thermo shaker at a speed of 100 rpm for a given time. The suspensions were centrifuged at 2500 rpm for 5 min and filtered. The equilibrium concentration MB in supernatant liquor was analyzed by standard colorimetric method using UV–visible spectrophotometer (Shimadzu UV-1601) at 620 nm. The pH of the sample was adjusted using 0.1 N HCl or 0.1 N NaOH solution. The percentage metal ion removal and amount of metal ion adsorbed per unit mass of adsorbent q_e (mg/g) were obtained using following equations (Gupta et al., 2010):

$$R = \frac{C_0 - C_e}{C_0} \times 100 \quad (1)$$

$$q_e = (C_o - C_e)\frac{V}{M} \quad (2)$$

where C_0 and C_e are the initial and equilibrium concentrations of MB dye (mg/L), V is the volume of the solution (L), and M is the mass of the adsorbent used (g).

2.4. Instrumentation

X-ray diffraction data were recorded using a Phillips (Holland), model PW 1148/89 X-ray diffractometer. Fourier transformer infrared spectra (FTIR) were obtained using Perkin Elmer spectrometer (Spectrum 400, USA). The surface morphology of nanocomposite was studied using scanning electron microscope (SEM Quant-250, model 9393). The microstructure was analyzed by transmission electron microscopy (TEM) using Tecnai 20 G2 (Plate/CCD Camera). The dye concentration was determined using Systronics 117 UV–visible spectrophotometer.

2.5. Ion exchange activity of GG/CTNC

2.5.1. Ion exchange capacity

0.5 g (dry mass) of GG/CTNC in H^+ form was placed in a glass tube of 1 cm internal diameter at glass wool supported at the bottom. The column containing GG/CTNC was washed with double distilled water to remove excess acid. 0.1 M NaCl (250 mL) solution was used as eluant to elute the H^+ from GG/CTNC. The flow rate of eluant was maintained at 0.5 mL min^{-1}. The collected effluent was titrated against a standard alkali solution using phenolphthalein as an indicator. The hydrogen ions released were calculated using the formula as (Siddiqui, & Khan, & Inamuddin, 2007):

$$\text{IEC} = \frac{N \times V}{W} \text{ mequiv } g^{-1} \quad (3)$$

where IEC is ion exchange capacity. N and V (mL) are normality and volume of NaOH, respectively. W (mg) is the weight of GG/CTNC.

2.5.2. Thermal stability

0.5 g sample of GG/CTNC in H^+ form was heated at different temperatures in muffle furnace for 1 h. The sample was weighed and ion exchange capacity was determined after cooling them at room temperature by method as described above.

2.5.3. Effect of eluant concentration

The optimum concentration of the eluant for complete elution of H^+ ions from CA/ZPNC was studied. 250 mL of $NaNO_3$ solution of different concentration was passed through the columns, containing 0.5 g of the exchanger in H^+ form with a flow rate of 0.5 mL min^{-1}. The collected effluents were titrated against 0.1 M NaOH to determine the eluted H^+ ions.

2.5.4. Elution behavior

$NaNO_3$ solution (1 M) was passed through a column containing 0.5 g of GG/CTNC for complete elution of H^+. Effluent was collected in 10 mL fraction at a flow rate of 0.5 mL min^{-1}. Each fraction of 10.0 mL was titrated against 0.1 M NaOH solution.

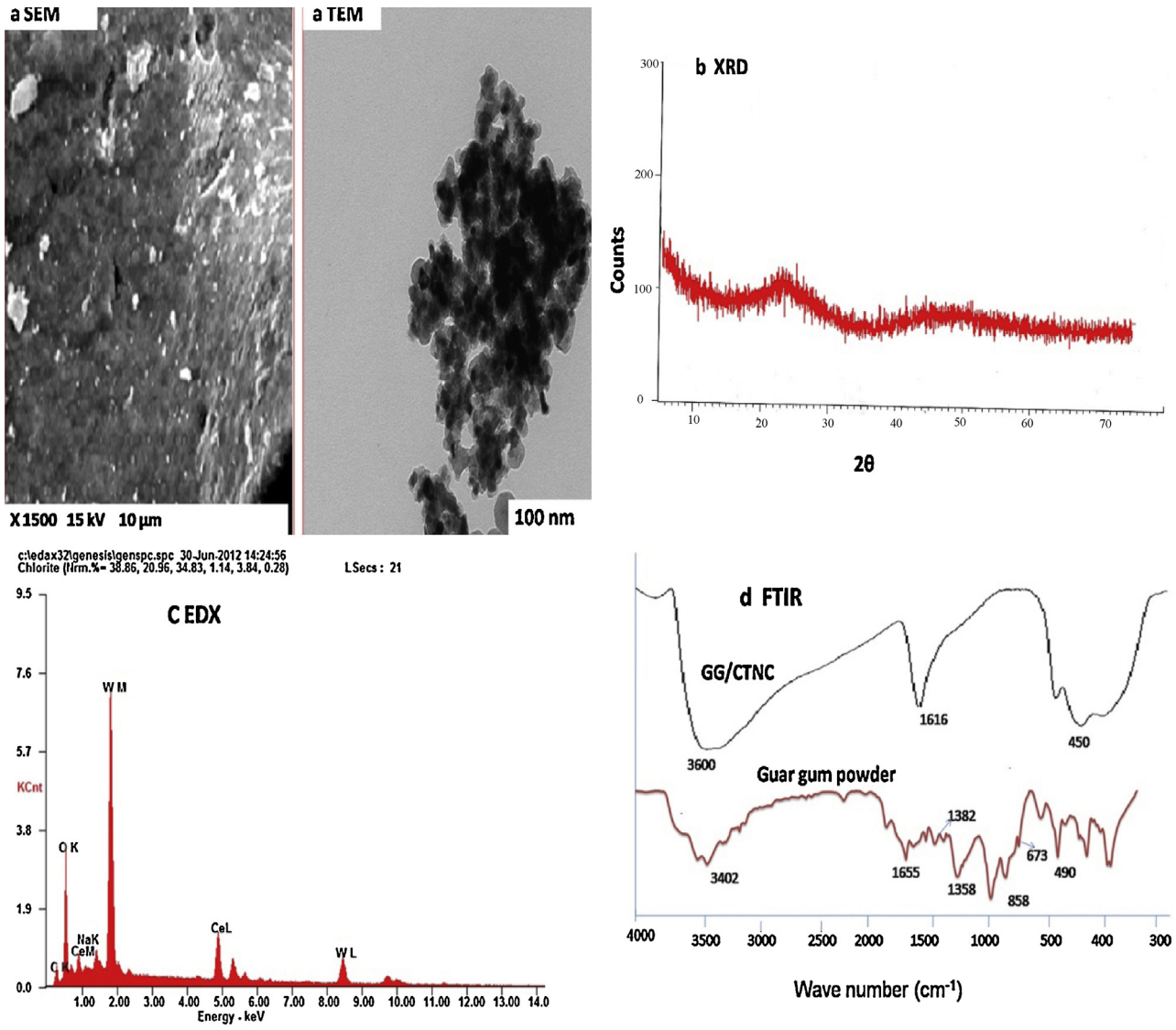

Fig. 1. (a) SEM and TEM images of GG/CTNC. (b) XRD study of guar gum–cerium (IV) tungstate composite. (C) EDX spectrum of gaur gum–cerium (IV) tungstate nanocomposite (GG/CTNC). (d) FTIR spectra of guar gum and GG/CTNC.

2.5.5. pH-titration

In typical method, 0.5 g of GG/CTNC in H^+ form was placed in each 250 mL conical flask containing equimolar solutions of alkali metal chlorides and their hydroxide in different volume ratios. Total volume was kept 50 mL to make ionic strength constant. The pH of the solution was recorded every 24 h until equilibrium is attained which needed 10 days.

2.5.6. Distribution studies

Distribution coefficients of different metal ions such as Pb^{2+}, Zn^{2+}, Th^{2+}, Cu^{2+}, Ni^{2+}, Cd^{2+}, Mg^{2+} were determined in aqueous solution using batch process. 0.5 g of GG/CTNC in H^+ form and 20 mL of different metal nitrate solutions were continuously shaken for 24 h at 25 °C. Metal ion concentration was determined by titrating against standard EDTA solution. K_d values (mL/g) were determined using following formula:

$$K_d = \frac{I - F}{F} \times \frac{V}{M} \text{ mL/g} \quad (4)$$

where I and F indicate initial and final concentration of metal ion in solution. V and M denotes final volume of the solution (mL) and amount of ion exchanger (g), respectively.

3. Results and discussion

3.1. Characterization

Fig. 1a (SEM) depicts scanning electron microscopy (SEM) images of guar gum–cerium tangstate nanocomposite (GG/CTNC). GG/CTNC exhibits rough surface with different sized particles to form microsphere. TEM images signify homogeneous distribution of guar gum (GG) and cerium (IV) tungstate particles (CT) in nanocomposite (Fig. 1a (TEM)). The darker portion signifies GG wrapped CT while gray part shows free GG in polymeric backbone. The high level formation of GG/CTNC can be seen in TEM image. The size of GG/CTNC was observed to be 50 nm.

Fig. 1b represents X-ray diffraction pattern of GG/CTNC. The broader diffraction peaks between 10° and 23° clearly were clearly seen in GG/CTNC (Gupta et al., 2012). The low intensity broader peaks indicated the amorphous nature of GG/CTNC. EDX studies confirms that Ce, W, O, C elements are present in weight percentage of 21, 25, 40 and 9, respectively (Fig. 1c).

FTIR spectra of gaur gum and GG/CTNC were shown in Fig. 1d. The presence of a strong absorption band at 3402 cm^{-1} indicated —OH bond stretching vibration. The absorption band due to

Table 1
Effect of temperature on ion exchange capacity of guar gum–Ce (IV) tungstate composite exchanger.

Heating temperature (°C)	Wt. of ppts before heating (g)	Wt. of ppts after heating (g)	IEC for Na^+ ion (mequiv g^{-1})	Retention of ion exchange capacity
75	0.53	0.48	1.30	92.85
100	0.53	0.47	1.28	91.42
200	0.53	0.41	0.82	58.57
300	0.53	0.40	0.64	45.71
400	0.53	0.35	0.42	30.00

ring stretching of mannose may be appeared at 1655 cm^{-1}. The absorption bands recorded at 1382 and 1358 cm^{-1} may due to symmetrical deformations of —CH_2 and —COH groups. The weak band at 673.71 cm^{-1} corresponds to ring stretching and ring deformation of α-D-(1-4) and α-D-(1-6) linkages (Chauhan, Chauhan, & Ahn, 2009). In FTIR spectrum of GG/CTNC, the broad band at 3600 cm^{-1} corresponds to loosely free –OH group. The strong and broad band at 3360 cm^{-1} may be due to free —OH group. The shift in the absorption frequency from 1655.96 cm^{-1} to 1616.31 cm^{-1} confirmed the interaction of guar gum with Ce (IV) tungstate (Brigante & Schulz, 2012).

3.2. Ion exchange behavior of GG/CTNC

The maximum ion-exchange capacity of the 'GG/CTNC was found to be 1.3 mequiv g^{-1} for Na^+ ions. The improved ion exchange capacity of GG/CTNC exchanger was due to the binding of polymeric material with inorganic moiety. The nano hybrid exchanger exhibited good reproducible characteristic. Under identical conditions (pH 2, dosage = 0.5 g and reaction time = 24 h), GG/CTNC did not show any appreciable change in the percentage of yield and ion exchange capacity.

Table 1 shows the effect of temperature on the ion exchange capacity of GG/CTNC exchanger. It was revealed that ion exchange capacity decreased with increase in temperature. GG/CTNC was quite stable and retained about 30% ion exchange capacity even upto 400 °C. The effect of eluant concentration on ion exchange capacity of GG/CTNC was investigated (Fig. 2a). The rate of elution was governed by the concentration of the eluant used onto the composite ion exchange materials (Inamuddin et al., 2007; Siddiqui et al., 2007). The optimum concentration of $NaNO_3$ as eluant was found to be 1 M for the maximum release of H^+ ions from GG/CTNC.

Fig. 2b depicts the pH titration behavior of GG/CTNC with NaOH–NaCl system. The pH titration result confirmed the monofunctional nature of nanocomposite. GG/CTNC behaved as strong cation exchanger as indicated by low pH of solution when no OH^- ions were added.

The distribution studies showed that GG/CTNC exchanger was found to be highly selective for Pb^{2+} as compared to other metal ions. Thus the composite ion exchanger can be utilized for the determination and separation of lead ions from waste effluents.

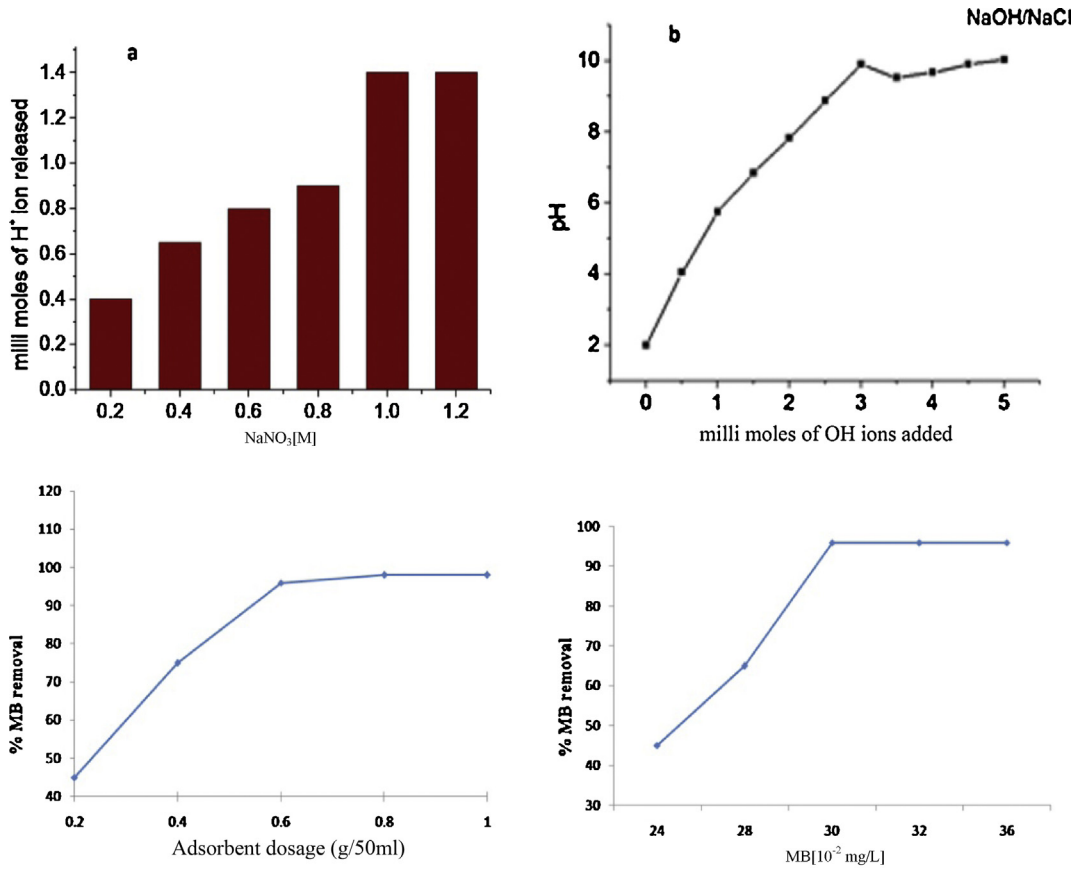

Fig. 2. (a) Effect of eluent concentration on ion exchange capacity of GG/CTNC exchanger. (b) pH titration curves for GG/CTNC exchanger. (c) Effect of adsorbent dosage on MB removal: (MB concentration = 0.32 mg/L, contact time= 120 min, pH 9, temperature = 30 ± 1 °C). (d) Effect of initial dye on MB removal [adsorbent dose = 0.4 g/50 ml, contact time = 120 min, pH 9, temperature = 30 ± 1 °C).

The order of selectivity for different metal ions were observed as Pb (K_d = 223) Zn (K_d = 189) > Th (K_d = 90) > Cu (K_d = 65.7) > Ni (K_d = 61.0) > Cd (K_d = 59.17) > Mg (K_d = 41.5).

3.3. Effect of reaction parameter on adsorption ability of methylene blue onto GG/CTNC

The effect of adsorbent dosage on MB removal was studied at pH 9 and ambient temperature (30±1 °C). It is evident from Fig. 2c that the removal of MB increased sharply with increase in adsorbent dose from 0.2 g/50 mL to 0.4 g/50 mL. It was due to the reason that the increased adsorbent dose resulted in an increase in mass gradient between the solution and adsorbent. Beyond 0.4 g/50 mL of adsorbent loading, there was no significant change in percentage removal of MB. Therefore, due to conglomeration of adsorbent particles, increase in effective surface area of adsorbent was negligible (Gupta et al., 2007). So, 0.4 g/50 mL was considered as optimal adsorbent dosage for GG/CTNC loading and was used for further study.

Adsorption efficiency was increased with increase in MB concentration from 0.24 mg/L to 0.32 mg/50 mL (Fig. 2d). At lower MB concentration, the unoccupied active sites on the adsorbent surface were higher for adsorption. However, beyond 0.32 mg/L of MB concentration, the number of active sites for adsorption of was lowered due to occupation of activated site of adsorbents by dye molecule. Therefore, further increase in MB concentration did not indicate any significant adsorption (Constantin et al., 2013; Gupta et al., 2007).

The effect of contact time on MB removal was shown in Fig. 3a. It has been clear from Fig. 3a that about 96% dye was removed in 120 min of contact time. No significant changes in removal efficiency were observed after 120 min. The change in rate of adsorption might be due to fact that initially all the adsorbent sites were vacant and solute concentration gradient is very high. Later, the decreased vacant sites of adsorbent resulted in lowering of adsorption due to monolayer formation of MB adsorbent surface (Constantin et al., 2013; Gupta et al., 2007). So, the adsorption equilibrium was attained after 120 min of contact time for MB adsorption.

Percentage removal of MB using GG/CTNC was investigated at different solution pH. The obtained results were presented in Fig. 3b. It has been revealed that the MB removal was increased with pH from 2 to 9. It was due to reason that on increasing pH, the surface charge of adsorbent became more and more negatively. It resulted in higher force of attraction between cationic MB and negatively charged adsorbent surface ultimately leading to higher MB adsorption (Bhattacharyya & Sharma, 2005; Dogan, Alkan, Turkyilmaz, & Ozdemir, 2004).

3.4. Isotherm data analysis

The adsorption isotherms revealed the specific relationship between adsorbate concentration in the bulk and adsorbed amount at interface. In this study, equilibrium data was modeled by using Langmuir, Freundlich and Tempkin isotherm equations (Gupta et al., 2007; Dogan et al., 2004). Langmuir isotherm was given by following equation (Langmuir, 1918):

$$\frac{C_e}{q_e} = \frac{1}{bq_0} + \frac{1}{b} C_e \tag{5}$$

where q_e is amount of adsorbate adsorbed per unit weight of adsorbent (mg/g), q_0 is the monolayer adsorption capacity (mg/g), C_e is the initial concentration(mg/L) and b is the Langmuir constant (L/mg). In order to determine the feasibility of adsorption process,

Table 2
Isotherm model for MB adsorption onto GG/CTNC.

Models	Isotherm constants			
Langmuir	q_m (mg/g)	b (L/mg)	R_L	R^2
	120.68	3.25	0.918	0.99
1.14	0.593	K_f (mg/g)	–	R^2
A (L/g)	–		–	0.93
Temkin			B	R^2
	0.058	–	530	0.98

dimensionless constant separation term (R_L) may be expressed as (Gupta et al., 2010):

$$R_L = \frac{1}{1 + bC_e} \tag{6}$$

The obtained R_L values ($0 < R_L < 1$) favored the adsorption of MB onto adsorbents. From Table 2 and Fig. 3c, the value of correlation coefficients was very high, indicating a good fit of monolayer Langmuir model to the adsorption of MB by GG/CTNC (Bhattacharyya & Sharma, 2005; Dogan et al., 2004).

Freundlich isotherm model was given by following equation (Freundlich, 1906):

$$\log q_e = \log K_f + \frac{1}{n} \log C_e \tag{7}$$

where adsorbate K_f and q_e are Freundlich adsorption constants, which can be determined by the linear plot of $\log q_e$ and $\log C_e$. The value of correlation coefficient (R^2) was observed to be 0.93. MB adsorption onto GG/CTNC did not follow Freundlich isotherm model closely. The value of n more than unity (1.14) was an indication of significant adsorption onto the adsorbent (Bhattacharyya & Sharma, 2005; Dogan et al., 2004).

Temkin isotherm assumes that heat of adsorption of all the molecules in the layer decreases linearly with coverage due to adsorbent-adsorbate interactions (Temkin & Pyzhev, 1940). The following equation represents Tempkin isotherm model.

$$\log\ q_e = \beta\ \ln \alpha + \beta\ \ln\ C_e \tag{8}$$

where $\beta = (RT)/b$, T is absolute temperature in Kelvin and R is universal gas constant, 8.314 J $(\text{mol K})^{-1}$. The adsorption data was analyzed according to the linear form of Temkin isotherm. The linear regression R^2 (0.987) was higher than Frendlich isotherm model (Table 2). Therefore, MB adsorption onto GG/CTNC followed Tempkin isotherm closely than Frendlich isotherm (Gupta & Ali, 2008).

3.5. Adsorption kinetics

The kinetic study was important to describe the time dependence of system under various conditions. The pseudo first order rate constant was given by following equation (Ho & McKay, 1999; Zacar & Engil, 2004):

$$\log (q_e - q_t) = \log\ q_e - \frac{k_1}{2.303}\, t \tag{9}$$

where q_t and q_e are the adsorption capacities at contact time and at equilibrium time, respectively. k_1 is rate constant for adsorption process.

The pseudo second order rate equation was described by following equation (Gupta et al., 2010; Ho & McKay, 1999; Zacar & Engil, 2004):

$$\frac{t}{q_e} = \frac{1}{k_2 q_e^2} + \frac{t}{q_e} \tag{10}$$

where k_2 is rate constant of pseudo second order equation (g/mg min). The value q_e and q_t are the adsorption capacity at equilibrium and at time t, (mg/g) respectively.

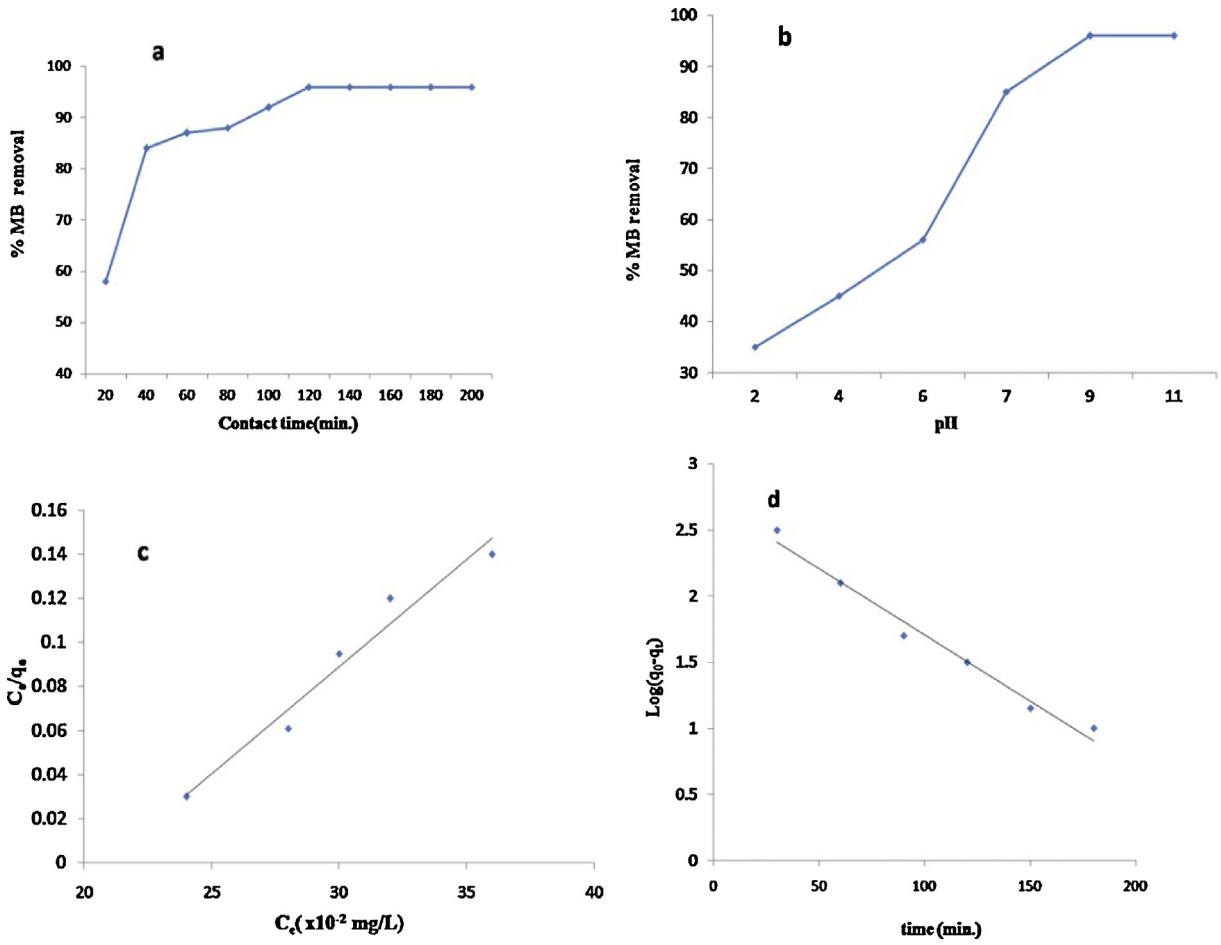

Fig. 3. (a) Effect of contact time on MB removal. (MB concentration = 0.32 mg/L, adsorbent dose = 0.4 g/50 ml, pH 9, temperature = 30 ± 1 °C). (b) Effect of pH on MB removal. (MB concentration = 0.32 mg/L, adsorbent dose = 0.4 g/50 ml, contact time = 120 min., temperature = 30 ± 1 °C). (c) Langmuir adsorption isotherm for MB removal. (d) Pseudo first order kinetics for MB removal.

The pseudo second order kinetics was fitted well with the experimental data as compared to pseudo first order kinetics (Figs. 3a and 4a and Table 3). The correlation coefficients were in good agreement with pseudo second order kinetic models ($R^2 > 0.99$) (Table 3). The high value of R^2 and applicability of pseudo second kinetics indicated that the adsorption process was enhanced by chemisorptions (Fig. 4 and Table 3). So, chemisorption was the rate-controlling mechanism for the adsorption process (Gupta et al., 2010; Ho & McKay, 1999; Zacar & Engil, 2004).

The possibility of intraparticle diffusion was determined by using following equation (Gupta et al., 2007):

$$q_t = k_{id} t^{1/2} + C \quad (11)$$

where C is intercept and K_{id} is intraparticle diffusion rate constant (mg/L min$^{1/2}$). Plot of q_t versus $t_{1/2}$ should be linear if intraparticle diffusion is involved in the adsorption process. The results of intraparticle diffusion were shown in Fig. 4b and Table 4. The linear portion of the plot did not pass through origin. This deviation from the origin was due to the variation of mass transfer in the initial and final stages of adsorption. The adsorption process occurred in two or more steps. At final equilibrium stage, the intraparticle diffusion slowed down due to saturation of adsorbent and MB was slowly transported into the pores and retained in the micropores (Bhattacharyya & Sharma, 2005; Dogan et al., 2004). The adsorption process has not obeyed the intraparticle diffusion model.

Table 3
Kinetic model for MB adsorption onto GG/CTNC.

Pseudo first order model			
k_1 (min^{-1})	q_e (exp.)	q_e (mg/g)	R^2
0.0230	120.68	100.17	0.94
Pseudo second order model			
k_2 (g/mg min)	q_e (mg/g)		R^2
0.00125	118.305		0.99
Intraparticle diffusion model			
K_{id} (mg/g min$^{1/2}$)	C (mg/g)		R^2
0.682	3.134		0.893

3.6. Effect of temperature and adsorption thermodynamics

The effect of temperature on the adsorption was investigated under optimized conditions (Fig. 4c). It was observed that adsorption of MB decreased with increase in temperature from 303–343 K. The decrease in adsorption capacity with temperature was due to

Table 4
Thermodynamic parameters for MB adsorption at temperature range of 303–343 K.

Temperature (K)	ΔG (KJ/mol)	ΔH (KJ/mol)	ΔS (KJ/K mol)
303	−0.95	3.66	0.044
313	−1.35	3.00	0.04
323	−2.85	2.75	0.035
333	−4.25	2.35	0.030
343	−5.27	2.00	0.027

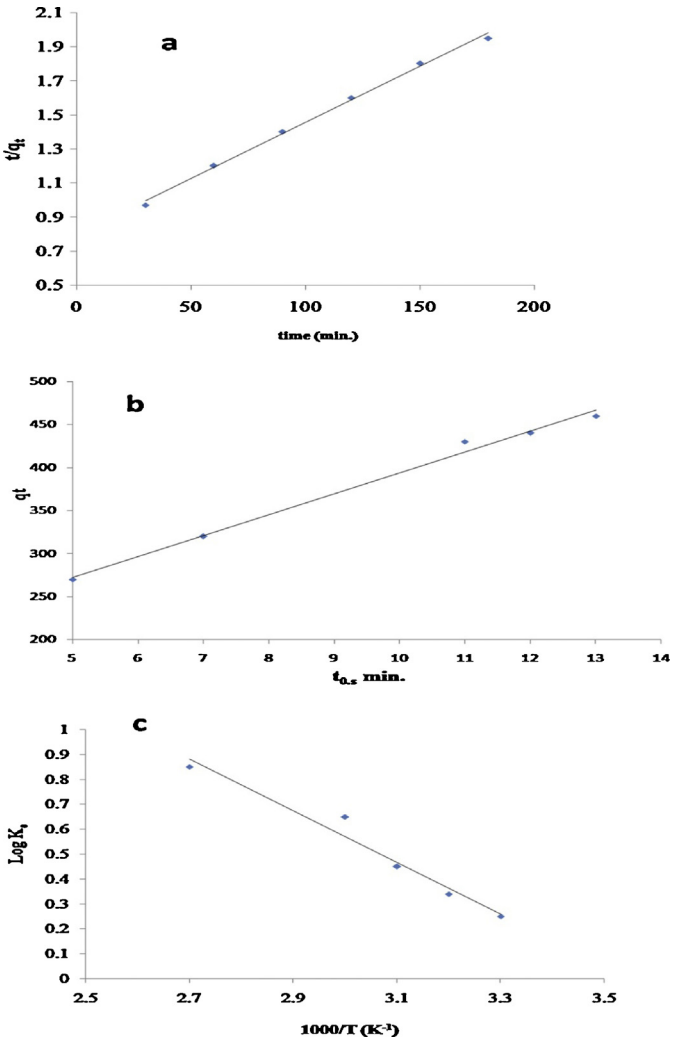

Fig. 4. (a) Pseudo second order kinetics for MB removal. (b) Intraparticle diffusion plot for MB removal. (c) Effect of temperature on MB adsorption. (MB concentration = 0.32 mg/L, adsorbent dose = 0.4 g/50 ml, contact time = 120 min, pH 9).

the weakening of the adsorptive forces between the active sites of adsorbent surface and adsorbate (Arami, Limaee, & Mahmoodi, 2008). The main criterion which leads to a chemisorption or physisorption was the determination of the enthalpy ΔH. Thermodynamic parameters such as Gibbs free energy (ΔG), enthalpy (ΔH) and entropy (ΔS) were given by using the following equations (Arami et al., 2008; Gupta & Ali, 2008).

$$\Delta G = -RT\ln(K_c) \tag{12}$$

$$\Delta G = \Delta H - T\Delta S \tag{13}$$

$$\log K_c = \frac{\Delta S}{R} - \frac{\Delta H}{2.303}RT \tag{14}$$

where K_c is the equilibrium constant of the adsorption and may be defined as:

$$K_c = \frac{C_{\text{adsorbent}}}{C_{\text{solution}}} \tag{15}$$

where $C_{\text{adsorbent}}$ and C_{solution} are the concentration of MB onto the adsorbents and residual MB concentration at adsorption–desorption equilibrium. The value of enthalpy (ΔH) and entropy (ΔS) were calculated from the slope and intercepts of the plot of $\log K_c$ versus $1/T$ (Fig. 4c). Table 4 shows the thermodynamic parameters for the adsorption MB onto GG/CTNC. The negative value of Gibbs free energy indicated the spontaneous nature of adsorption process and the degree of spontaneity of the reaction increased with increase in temperature (Table 4). Adsorption process seemed to be endothermic in nature. These results supported that adsorption mechanism was primarily chemisorptions. The positive value of ΔS suggested the increased randomness at the solid-solution interface due to the redistribution of energy between adsorbent and adsorbate during adsorption process. In the beginning of adsorption process, adsorbate ions were heavily solvated and the system became more ordered. However, the order was lost when the ions were adsorbed on the surface due to the release of solvated water molecules.

4. Conclusion

Guar gum–Ce (IV) tungstate was prepared by sol gel method. Ion exchange capacity of hybrid ion exchanger for Na^+ ion was noted to be 1.3 mequiv g^{-1}. pH titrations indicated the mono functional nature of GG/CTNC. Spectral studies confirmed the formation of GG/CTNC. Guar gum based ion exchanger was highly selective for lead metals. Optimization of different parameters such as dosage, initial dye concentration and contact time for adsorption of methylene blue dye was studied. The optimum parameters for adsorption of MB onto GG/CTNC was found to be MB concentration 0.32 mg/L, adsorbent dose 0.4 g/50 mL, contact time 120 min, temperature $30 \pm 1\,^{\circ}C$. The adsorption of MB followed pseudo first second order kinetics. The adsorption studied showed the endothermic nature of adsorption process. This study revealed the applicability of GG/CTNC for environmental remediation involving the dye removal from aqueous phase.

References

Arami, M., Limaee, N. Y., & Mahmoodi, N. M. (2008). Evaluation of the adsorption kinetics and equilibrium for the potential removal of acid dyes using a biosorbent. *Chemical Engineering Journal*, *139*, 2–10.

Bhattacharyya, K., & Sharma, A. (2005). Kinetics and thermodynamics of methylene blue adsorption on neem leaf powder. *Dyes and Pigments*, *66*, 51–59.

Brigante, M., & Schulz, P. C. (2012). Adsorption of the antibiotic minocycline on cerium(IV) oxide: Effect of pH, ionic strength and temperature. *Microporus and Mesoporous Materials*, *156*, 138–144.

Chauhan, K., Chauhan, G. S., & Ahn, J. H. (2009). Synthesis and characterization of novel guar gum hydrogel and their use as Cu (II) sorbent. *Bioresource Technology*, *100*(3), 3599–3603.

Constantin, M., Asmarandei, I., Harabagiu, V., Ghimici, L., Ascenzi, P., & Fundueanu, G. (2013). Removal of anionic dyes from aqueous solutions by an ion-exhanger based on pullulan microsphere. *Carbohydrate Polymers*, *91*, 74–84.

Dogan, M., Alkan, M., Turkyilmaz, A., & Ozdemir, Y. (2004). Kinetics and mechanism of removal of methylene blue by adsorption onto perlite. *Journal of Hazardous Materials*, *109*, 141–148.

Dong, F., Sun, Y., Min, F., Wu, Z., & Lee, S. C. (2012). Room temperature synthesis and highly enhanced photocatalytic activity of porous BiOI/BiOCl composites nanoplates microflowers. *Journal of Hazardous Materials*, *219*, 26–34.

Freundlich, H. M. F. (1906). Over the adsorption in solution. *Journal of Physical Chemistry*, *57*, 385–471.

Gupta, V. K., & Ali, I. (2008). Removal of endosulfan and methoxychlor from water on carbon slurry. *Environmental Science and Technology*, *42*, 766–770.

Gupta, V. K., Jain, R., & Varshney, S. (2007). Removal of reactofix golden yellow 3 RFN from aqueous solution using wheat husk – An agricultural waste. *Journal of Hazardous Materials*, *142*, 443–448.

Gupta, V. K., Mittal, A., Malviya, A., & Mittal, J. (2009). *Adsorption of carmoisine A from wastewater using waste materials—Bottom ash and deoiled soya*, *335*, 24–33.

Gupta, V. K., Rastogi, A., & Nayak, A. (2010). Biosorption of nickel onto treated alga (*Oedogonium hatei*): Application of isotherm and kinetic models. *Journal of Colloid and Interface Science*, *342*, 533–539.

Gupta, V. K., Agarwal, S., & Saleh, T. A. (2011). Chromium removal by combining the magnetic properties of iron oxide with adsorption properties of carbon nanotubes. *Water Research*, *45*, 2207–2212.

Gupta, V. K., Pathania, D., Agarwal, S., & Singh, P. (2012). Preparation of cellulose acetate-zirconium (IV) phosphate nanocomposite with ion exchange capacity and enhanced photocatalytic activity. *Journal of Hazardous Materials*, *243*, 179–186.

Ho, Y. S., & McKay, G. (1999). Pseudo-second order model for sorption processes. *Process Biochemistry*, *34*, 451–465.

Huang, S. H., & Chen, D. H. (2009). Rapid removal of heavy metals cations and anions from aqueous solution by an amino-fucntionalized magnetic nano-adsorbent. *Journal of Hazardous Materials*, *163*, 174–179.

Inamuddin, Khan, S. A., Siddiqui, W. A., & Khan, A. A. (2007). Synthesis, characterization and ion-exchange properties of a new and novel 'organic–inorganic hybrid' cation-exhanger: Nylon-6,6, Zr(IV) phosphate. *Talanta*, *71*, 841–847.

Langmuir, I. (1918). The adsorption of gases on plane surfaces of glass, mica and platinum. *Journal of the American Chemical Society*, *40*, 1361–1403.

Mittal, A., Gupta, V. K., Malviya, A., & Mittal, J. (2008). Process development for the batch and bulk removal and recovery of a hazardous, water-soluble azo dye (Metanil Yellow) by adsorption over waste materials (Bottom Ash and De-Oiled Soya). *Journal of Hazardous Materials*, *151*, 821–832.

Mittal, A., Mittal, J., Malviya, A., Kaur, D., & Gupta, V. K. (2010). Adsorption of hazardous dye crystal violet from wastewater by waste materials. *Journal of Colloid and Interface Science*, *343*, 463–473.

Nevarez, L. M., Casarrubias, L. B., Canto, O. S., Celzard, A., Fierro, V., Gomez, R. I., et al. (2011). Biopolymers-based nanocomposites: Membranes from propionated lignin and cellulose for water pourification. *Carbohydrate Polymers*, *86*, 732–741.

Park, B. D., & Kadla, J. F. (2012). Thermal degradation kinetics of resole phenol-formaldehyde resin/multi-walled carbon/cellulose nanocomposite. *Thermochimica Acta*, *540*, 107–115.

Semischenko, K. B., Stepanenko, I. V., Gulina, L. B., & Tolstoi, V. P. (2011). Synthesis and study of cerium(IV) polytungstate nanolayers. *Russian Journal of General Chemistry*, *81*(6), 1075–1077.

Siddiqui, W. A., Khan, A. A., & Inamuddin, S. A. (2007). Synthesis, characterization and ion-exchange properties of a new and novel 'organic–inorganic hybrid' cation-exhanger: Poly(methylene methacrylate) Zr(IV) phosphate. *Colloids and Surfaces A*, *295*, 193–199.

Sivasankar, V., Murugesh, S., Rajkumar, S., & Darchen, A. (2013). Cerium dispersed in carbon (CeDC) and its adsorption behavior: A first example of tailored adsorbent for fluoride removal from drinking water. *Chemical Engineering Journal*, *214*, 45–54.

Temkin, M. J., & Pyzhev, V. (1940). Recent modification to Langmuir isotherms. *Acta Physicochimica*, *12*, 217–225.

Vilhera, C., Goncalves, M. L., & Mota, A. M. (2004). Binding of copper (II) to pectin by electromchemical methods. *Electroanalytical*, *16*, 2065–2072.

Virkutyte, J., Jegatheesan, V., & Varma, R. S. (2012). Visible light activated TiO_2/microcrystalline cellulose nanocatalyst to destroy organic contaminant in water. *Bioresource Technology*, *113*, 288–293.

Yang, Z., Chen, S., Hu, W., Yin, N., Zhang, W., Xiang, C., et al. (2012). Flexible luminescent CdSe/bacterial cellulose nanocomposite membrane. *Carbohydrate Polymers*, *88*, 173–178.

Zacar, M. O., & Engil, I. A. S. (2004). Application of kinetic models to the sorption of disperse dyes onto alunite. *Colloids and Surfaces A: Physicochemical and Engineering Aspects*, *42*, 105–113.

Zhao, X. T., Zeng, T., Li, X. Y., Hu, Z. J., Gao, H. W., & Xie, Z. (2012). Modeling and mechanism of the adsorption of copper ion onto natural bamboo sawdust. *Carbohydrate Polymers*, *89*, 185–192.

Zhao, X. T., Zeng, T., Hu, Z. J., Gao, H. W., & Zou, C. Y. (2012). Modeling and mechanism of the adsorption of proton onto natural bamboo sawdust. *Carbohydrate Polymers*, *87*, 1199–1205.